RSC Advances

PAPER

View Article Online
View Journal | View Issue

Check for updates

Cite this: *RSC Adv.*, 2024, **14**, 28716

Synthesis, mixed-spin-state structure and Langmuir–Blodgett deposition of amphiphilic Fe(III) quinolylsalicylaldiminate complexes†

Peeranuch Poungsripong,[b] Theerapoom Boonprab,[a] Phimphaka Harding,[a] Keith S. Murray,[c] Wasinee Phonsri,[c] Ningjin Zhang,[d] Jonathan A. Kitchen *[ef] and David J. Harding *[a]

Received 23rd August 2024
Accepted 4th September 2024

DOI: 10.1039/d4ra06111j

rsc.li/rsc-advances

Designing and integrating Fe(III)-based spin crossover (SCO) complexes onto substrates remains a challenging goal with only a handful of examples reported. In this work, we successfully synthesized and characterized three $[Fe(qsal\text{-}OR)_2]NO_3$ (qsal-OR = 5-alkoxy-2-[(8-quinolylimino)methyl]phenolate) complexes, in which R = $C_{12}H_{25}$ **1**, $C_{16}H_{33}$ **2**, and $C_{22}H_{45}$ **3** to explore the impact of alkyl chain on the modulation of SCO activity and potential for self-assembly on a glass surface. The SCO is found to be gradual and incomplete in all cases, with the LS state more stabilised as the alkyl group shortens. We also demonstrate that all complexes form stable Langmuir films and achieve good transfer ratios to the glass surface, with **2** being the best in terms of stability. This paves the way for the SCO modulation of complexes in this class and the development of SCO devices.

Introduction

The design of switchable molecules is essential to the development of molecular electronic systems.[1,2] While a number of different switches are possible, *e.g.* optical, thermal and mechanical, some of the most promising are magnetic switches. A particularly interesting group of magnetic switches are spin crossover (SCO) compounds. SCO systems exhibit a change in their spin state as the electrons rearrange within the d-manifold, often under thermal stimulus.[3–6] An advantage of SCO materials is that they can also be switched under pressure, optically, or by introduction of guest molecules. In the case of Fe(III), the two spin states, high spin (HS, $S = 5/2$) and low spin (LS, $S = 1/2$) are both paramagnetic. This has important consequences for the structural changes that accompany SCO with differences in Fe–ligand bond lengths of 0.10–0.13 Å in Fe(III), while *ca.* 0.20 Å is typical for the more widely studied Fe(II) systems.[6,7] Despite this, Fe(III) complexes show the largest magnetic response upon SCO and are often air stable. This latter point is especially useful in the development of devices based on SCO materials.

While SCO was first discovered in Fe(III),[6] until recently it was largely ignored as the smaller structural changes were thought to limit the chances of abrupt SCO. In 2001, Sato and co-workers reported a large, repeatable hysteresis of 70 K in $[Fe(qsal)_2]NCSe$ demonstrating that Fe(III) systems can be just as effective as Fe(II).[8,9] Nevertheless, it took a further 10 years before Fe(III) SCO compounds became more actively studied. There are now examples of symmetry-breaking,[10–17] stepped,[18–20] hysteretic,[8,21–23] and even photoswitchable SCO.[24–26] Our group has been especially interested in the $[Fe(qsal\text{-}X)_2]^+$ series of SCO complexes exploring solvent,[27,28] substituent[29–31] and anion effects.[32–35] The success in many of these systems arises from careful control of the supramolecular interactions that link the spin centres. However, control over the SCO temperature, the type of SCO and the presence of hysteresis remains poor. Another problem is the challenge of immobilising SCO molecules onto surfaces, which is vital for tangible applications.

In seeking to address these challenges, we have taken inspiration from the work of Albrecht *et al.* who explored the impact that long alkyl chains have in $[Fe(4\text{-}OR\text{-}sal_2trien)]^+$ on the abruptness of SCO in solution.[36,37] In a series of papers, they demonstrated that longer alkyl chains give rise to increasingly abrupt SCO. Moreover, they were able to show that the complexes do self-assemble to form thin films. However, transfer of the films to a support proved difficult and transfer ratios were generally low,[38] limiting the use of these particular

[a]*School of Chemistry, Institute of Science, Suranaree University of Technology, Nakhon Ratchasima, 30000, Thailand. E-mail: david@g.sut.ac.th*

[b]*Functional Materials and Nanotechnology Center of Excellence, Walailak University, Thasala, Nakhon Si Thammarat, 80160, Thailand*

[c]*School of Chemistry, Monash University, Clayton, VIC, 3800, Australia*

[d]*School of Chemistry, University of Southampton, University Road, Southampton, SO17 1BJ, UK*

[e]*Department of Chemistry, Auckland University of Technology, New Zealand. E-mail: jonathan.kitchen@aut.ac.nz*

[f]*The MacDiarmid Institute for Advanced Materials and Nanotechnology, New Zealand*

† Electronic supplementary information (ESI) available. CCDC 2357075 and 2357074. For ESI and crystallographic data in CIF or other electronic format see DOI: https://doi.org/10.1039/d4ra06111j

Open Access Article. Published on 10 September 2024. Downloaded on 8/18/2025 3:56:59 AM. This article is licensed under a Creative Commons Attribution-NonCommercial 3.0 Unported Licence.

© 2024 The Author(s). Published by the Royal Society of Chemistry

Open Access Article. Published on 10 September 2024. Downloaded on 8/18/2025 3:56:59 AM. This article is licensed under a Creative Commons Attribution-NonCommercial 3.0 Unported Licence.

compounds. Other groups have been more successful with alkyl chain functionalization of SCO Fe(II) complexes reported with a range of ligand scaffolds.[39–46] It was found that the magnetism and some degree of cooperativity were retained in the film, but the detailed studies of the effect of these chains were not widely evaluated. More recent studies on alkylated Fe(II)[47–56] and Co(II)[57–59] complexes reveal that there can sometimes be a significant correlation between chain length and the SCO temperature, $T_{1/2}$ (ref. 52) and abruptness.[53]

We have previously reported that $[Fe(qsal\text{-}5\text{-}OMe)_2]^+$ complexes do undergo SCO while the structurally related $[Fe(qsal\text{-}4\text{-}OMe)_2]^+$ systems are invariably HS.[29] Consequently, in this work we sought to answer two questions. Firstly, do $[Fe(qsal\text{-}4\text{-}OR)_2]^+$ compounds (Fig. 1) with long alkyl chains undergo SCO and how does the length of the chain impact the completeness of the transition? Secondly, do these form thin films and how does the change in the head group on the Fe(III) centre influence the stability and transferability of the films relative to $[Fe(4\text{-}OR\text{-}sal_2trien)]^+$.[37] Our results show that not only do the long alkyl chains change the packing permitting SCO, but they also permit self-assembly forming stable films that can be readily transferred to glass substrates.

Results and discussion

Ligand synthesis and characterisation

Ligands Hqsal-$OC_{12}H_{25}$, Hqsal-$OC_{16}H_{33}$ and Hqsal-$OC_{22}H_{45}$ were synthesised by the same general procedure (Scheme 1) reacting a stoichiometric amount of 8-aminoquinoline with 4-(dodecyloxy)salicylaldehyde, 4-(hexyloxy)salicylaldehyde or 4-(docosyloxy)salicylaldehyde at room temperature in DCM with trifluoroacetic acid as a catalyst. Following the reaction, evaporation to dryness and washing with hexane and diethylether resulted in yellow solids in good yields (83–99%). The ligands were fully characterised using ^{1}H NMR, IR, and UV/vis spectroscopy, mass spectrometry and where possible X-ray crystallography (see ESI†). All spectroscopic data was consistent with the formation of the desired ligands, although trace amounts of the starting aldehyde are present in all cases. Small yellow plate-like single crystals of Hqsal-$OC_{12}H_{25}$ were obtained by slow evaporation from a DCM solution. Hqsal-$OC_{12}H_{25}$ crystallized in the triclinic space group, $P\bar{1}$, with two crystallographically independent molecules of Hqsal-$OC_{12}H_{25}$ and one water molecule (disordered over two sites) in the asymmetric unit

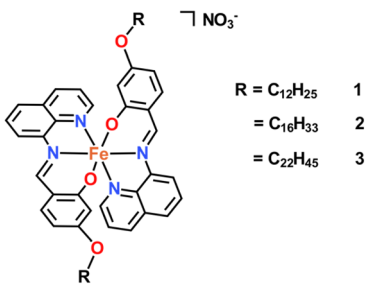

Fig. 1 Structure of complexes studied in this work.

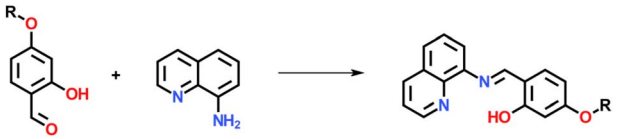

Scheme 1 Synthesis of Hqsal-OR.

(Fig. S14†). Both molecules of Hqsal-$OC_{12}H_{25}$ crystallize as the keto-amine tautomer [N2⋯O1 = 2.593(2) Å, <(N2–H2⋯O1) = 138.4(2)°; and N102⋯O101 = 2.610(2) Å, <(N102–H102⋯O101) = 136.0(2)°]. One molecule of Hqsal-$OC_{12}H_{25}$ has the interstitial water molecule hydrogen bonding to the keto oxygen atom [N200⋯O101′ = 2.672(4) Å, <(N200–H20D⋯O101′) = 162.4(2)°]. The overall packing in Hqsal-$OC_{12}H_{25}$ shows some interdigitation of the alkyl chains (Fig. S14†) which is common for such amphiphilic compounds.[60]

Complex synthesis and characterisation

Complexation reactions of Hqsal-$OC_{12}H_{25}$, Hqsal-$OC_{16}H_{33}$ and Hqsal-$OC_{22}H_{45}$ were carried out by mixing DCM solutions of the ligand with methanolic solutions of $Fe(NO_3)_3\cdot 9H_2O$ and stirring for 10 minutes before adding triethylamine and stirring for a further hour. The resulting dark solution was evaporated and then dissolved in DCM before being eluted through an Al_2O_3 flashpad. Evaporation of the dark solution gave the complexes as dark purple solids in modest yields (54–74%). Mass Spectrometry (ESI+) data for all complexes showed the expected peaks and isotopic ratios for $[Fe(qsal\text{-}OC_{12}H_{25})_2]^+$, $[Fe(qsal\text{-}OC_{16}H_{33})_2]^+$ and $[Fe(qsal\text{-}OC_{22}H_{45})_2]^+$ with m/z values of 918.47, 1030.60 and 1198.79, respectively (Fig. S9–S11†). Comparison of the infrared spectra of the ligands and complexes shows a decrease in the position of the C=N stretch, from ~1620 to ~1600 cm^{-1}, indicative of complexation (Fig. S4 and S12†). The nitrate counterion stretch is observed around 1380 cm^{-1}. The IR spectra of all complexes are in agreement with those of the related compounds, $[Fe(qsal\text{-}4\text{-}OMe)_2]^+$ confirming that the complexes have successfully formed (Fig. S12†).[29] The relative intensity of the aliphatic C–H stretching compared to the C=N also increases with alkyl chain elongation, confirming the integration of the chain into the molecule. Absorption spectra of all complexes in methanol showed intense absorption bands at 325 nm and 403 nm (Fig. S13†) most likely arising from π–π* and ligand-to-metal charge transfer (LMCT) transitions respectively.[29]

Powder X-ray diffraction studies reveal that the bulk materials are largely amorphous (Fig. S16†). Despite repeated attempts we have been unable to grow crystals of complexes **2** and **3**. However, single crystals of $[Fe(qsal\text{-}OC_{12}H_{25})_2]NO_3\cdot CH_2Cl_2$ were grown by evaporation from DCM and the structure determined at 100 K (Fig. 2). The compound crystallized in the triclinic space group $P\bar{1}$, and contained two molecules of $[Fe(qsal\text{-}OC_{12}H_{25})_2]NO_3$ and two interstitial DCM molecules in the asymmetric unit (Fig. S15†). Both complexes show the expected coordination to the Fe(III) centre where two ligands coordinate through the NNO coordination pocket at

Open Access Article. Published on 10 September 2024. Downloaded on 8/18/2025 3:56:59 AM. This article is licensed under a Creative Commons Attribution-NonCommercial 3.0 Unported Licence.

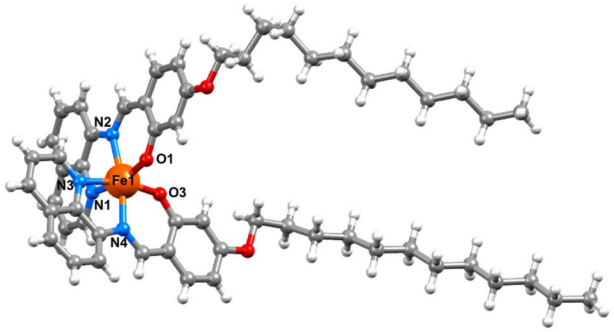

Fig. 2 View of the Fe1 molecule in $[Fe(qsal\text{-}OC_{12}H_{25})_2]NO_3 \cdot CH_2Cl_2$.

approximately 90° to each other and give distorted octahedral geometries with N_4O_2 coordination spheres. Analysis of the Fe–O and Fe–N bond lengths and angles showed that the two Fe(III) complexes adopt different spin states where Fe1–O = 1.883(3) Å, Fe1–N_{imine} = 1.931(4) and Fe1–$N_{quinoline}$ = 1.972(4) Å which are typical for LS Fe(III), and Fe2–O = 1.913(3) Å, Fe2–N_{imine} = 2.115(3) Å and Fe2–$N_{quinoline}$ = 2.137(4) Å, typical of the HS state (Table 1).[19,29] The octahedral distortion parameter (Σ) gave further evidence of the different spin states where Σ_{Fe1} = 49.6° and Σ_{Fe2} = 71.2°. While not unprecedented, [HS-LS] systems remain rare in Fe(III) SCO chemistry, with $[Fe(qsal\text{-}5\text{-}OMe)_2]Cl \cdot 2MeOH \cdot 0.5H_2O$ the most closely related example.[19] In contrast, $[Fe(qsal\text{-}4\text{-}OMe)_2]NO_3 \cdot CH_2Cl_2$ is entirely HS[29] and confirms that alkyl chains can be used to change the packing and enable SCO (*vide infra*). One alkyl chain on each complex adopts a trans co-planar arrangement while the other adopts a kink in the chain, this results in the chains being oriented in one direction relative to the Fe(III) centres, which gives an overall bi-layered packing arrangement with interdigitation of alkyl chains – an ideal conformation for Langmuir film formation (Fig. 3). These bilayer configurations and the kinks were also recognized in the SCO complexes for self-assembly application.[42,47,49,51,52,54,57,59,61] The 'head-groups' are linked to neighboring bi-layer headgroups through non-classical C–H hydrogen bonding interactions between aromatic C–H groups and the NO_3 counter anions (see Table S4 in the ESI†) as well as weak C–H$\cdots\pi$ stacking interactions [C106$\cdots$centroid$_{C32-C37}$ = 3.538 Å]. By comparison, $[Fe(4\text{-}OC_8H_{17}\text{-}sal_2trien)]PF_6$ also contains two independent Fe(III) centres in the asymmetric unit, but both are HS.[60] Moreover, unlike **1** the alkyl chains simply face each other with no evidence of interdigitation and the head groups are more loosely associated. Combined, this suggests that **1–3** should form more stable films.

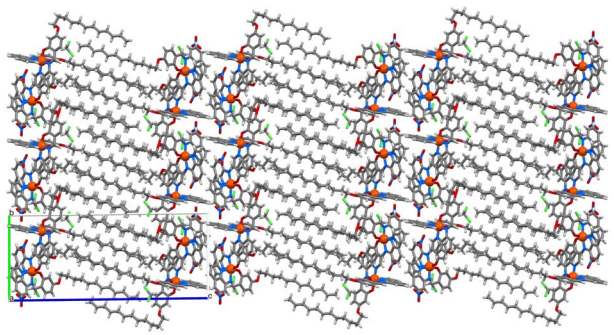

Fig. 3 Packing in **1** showing the formation of the bi-layers.

Scanning electron microscopy (SEM)

The morphologies of bulk samples of $[Fe(qsal\text{-}OR)_2]NO_3$ were evaluated by scanning electron microscopy (Fig. 4). Morphologies were found to heavily depend on the length of the alkyl chains, where $[Fe(qsal\text{-}OC_{12}H_{25})_2]NO_3$ existed as micro rods (Fig. 4a and b), $[Fe(qsal\text{-}OC_{16}H_{33})_2]NO_3$ appeared to have multiple morphologies and was observed as sheet-like plates (Fig. 4c), and spheres (Fig. 4d). The longest alkyl chain complex $[Fe(qsal\text{-}OC_{22}H_{45})_2]NO_3$ adopted a less structured morphology and exists as a network like structure (Fig. 4e and f) and is similar to that observed in $[Fe(4\text{-}OC_{22}H_{45}\text{-}sal_2trien)]NO_3$.[37] The alteration in morphologies as the alkyl-chain length changes is clear with more crystalline morphologies observed for the shorter chains.

Magnetic studies

Magnetic susceptibility studies of **1–3** were undertaken using SQUID magnetometry between 30–350 K with the SCO profiles shown in Fig. 5. The SCO is gradual in all cases, being most complete in $[Fe(qsal\text{-}OC_{12}H_{25})_2]NO_3$ with $\chi_M T$ increasing from *ca.* 2.0 cm^3 mol^{-1} K^{-1} at 30 K to 3.1 cm^3 mol^{-1} K^{-1} at 350 K. This is consistent with the structural data which show a [HS-LS] state at 150 K ($\chi_M T$ = 2.3 cm^3 mol^{-1} K^{-1}).

For the longer chain systems $\chi_M T$ increases by *ca.* 0.8 and 0.5 cm^3 mol^{-1} K^{-1}, for **2** and **3**, respectively. The changes in $\chi_M T$ represent *ca.* 29%, 21% and 13% SCO in **1**, **2** and **3**, respectively (assuming $\chi_M T$ = 0.40 cm^3 mol^{-1} K^{-1} for LS and $\chi_M T$ = 4.2 cm^3 mol^{-1} K^{-1} for HS). This suggests that as the alkyl chains become longer SCO becomes increasingly difficult, mirroring studies on dimeric Fe(II) SCO complexes.[48] It is also probable that the increasingly gradual and incomplete SCO reflects the lower crystallinity noted in the morphological studies. Interestingly, the SCO in **1–3** contrasts with $[Fe(4\text{-}OR\text{-}sal_2trien)]NO_3$ (R = C_6H_{13} to $C_{18}H_{37}$) which are entirely HS in the solid state,[60] indicating that the effect of the alkyl chains on SCO behaviour is dependent on the ligand system. Finally, we note that the presence of SCO in these longer chain systems, compared with the HS behaviour of $[Fe(qsal\text{-}4\text{-}OMe)_2]NO_3 \cdot CH_2Cl_2$,[29] confirms that the alkyl chains can be used to tune SCO characteristics.

Table 1 Fe–ligand bond lengths, angles and octahedral distortions parameters in **1** (Å, °)

	Fe1	Fe2
Fe–O	1.906(3), 1.918(3)	1.890(3), 1.871(3)
Fe–$N_{quin.}$	2.117(3), 2.156(4)	1.967(4), 1.975(3)
Fe–N_{imine}	2.115(3), 2.113(3)	1.928(4), 1.928(4)
cis-Bond angle range	76.5(2)–100.7(2)	83.1(2)–95.8(2)
trans-Bond angle range	163.9(2)–169.3(2)	175.9(2)–178.1(2)
Σ	70.9	52.7

© 2024 The Author(s). Published by the Royal Society of Chemistry

Open Access Article. Published on 10 September 2024. Downloaded on 8/18/2025 3:56:59 AM. This article is licensed under a Creative Commons Attribution-NonCommercial 3.0 Unported Licence.

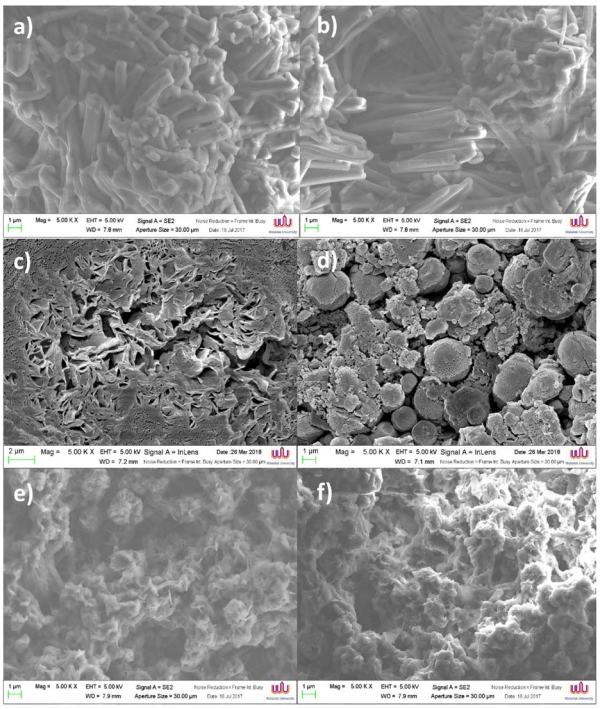

Fig. 4 SEM images of $[Fe(qsal\text{-}OC_{12}H_{25})_2]NO_3$ (a and b), $[Fe(qsal\text{-}OC_{16}H_{33})_2]NO_3$ (c and d) and $[Fe(qsal\text{-}OC_{22}H_{45})_2]NO_3$ (e and f).

Langmuir and Langmuir–Blodgett studies

The suitability of these amphiphilic systems for the formation of immobilized mono- and multi-layers was investigated by carrying out a full study of the Langmuir film forming abilities at an air–water interface. Pressure–area isotherms of Hqsal-$OC_{12}H_{25}$, Hqsal-$OC_{16}H_{33}$ and Hqsal-$OC_{22}H_{45}$ showed that, on pure water, the ligands all form Langmuir films with area per molecule values of 35, 25 and 20 Å^2 respectively and collapse pressures of 10, 25 and 45 mN m^{-1} respectively (Fig. S16†). These values are consistent with successful film formation,[62] however the low collapse pressure of Hqsal-$OC_{12}H_{25}$ indicates that the shorter 12-carbon chain system forms a somewhat weaker film. Time stability of the films was determined by holding the monolayers at a fixed molecular area and monitoring the surface pressure over a period of 10–15 minutes. The films showed reasonable stability over this timeframe, with only Hqsal-$OC_{22}H_{45}$ showing a slight decrease in surface pressure (Fig. S17†). Analogous studies were carried out for the corresponding Fe^{III} complexes.

All three complexes showed typical isotherms for the successful formation of ordered monolayers at the air–water interface where $[Fe(qsal\text{-}OC_{12}H_{25})_2]NO_3$ formed with an area per molecule value of 70 Å^2 and a film collapse pressure of 40 mN m^{-1}; $[Fe(qsal\text{-}OC_{16}H_{33})_2]NO_3$ formed with an area per molecule value of 85 Å^2 and a film collapse pressure of 45 mN m^{-1}; and $[Fe(qsal\text{-}OC_{22}H_{45})_2]NO_3$ formed with an area per molecule value of 85 Å^2 and a film collapse pressure of 50 mN m^{-1} (Fig. 6). Stability studies were again carried out to assess the suitability of these complexes for further deposition studies. The films were compressed to a pressure of 30 mN m^{-1} and the surface pressure monitored over time as the films were held static. Over a 20 minutes period, $[Fe(qsal\text{-}OC_{22}H_{45})_2]NO_3$ was found to form the most stable film with only a small decrease in surface pressure with the least stable film being formed by $[Fe(qsal\text{-}OC_{12}H_{25})_2]NO_3$. All films demonstrated sufficient stability for further deposition studies.

The ability of the Fe^{III} complexes to form highly ordered mono-layer films on quartz solid supports was investigated. Monolayer film depositions were investigated by vertical deposition of $[Fe(qsal\text{-}OR)_2]NO_3$ complexes onto quartz at surface pressures of 30 mN m^{-1}. Films were formed for all complexes with good transfer ratios (~1) on upstroke of the quartz slide – UV/vis measurements confirmed successful deposition of the highly coloured complexes (Fig. 7).

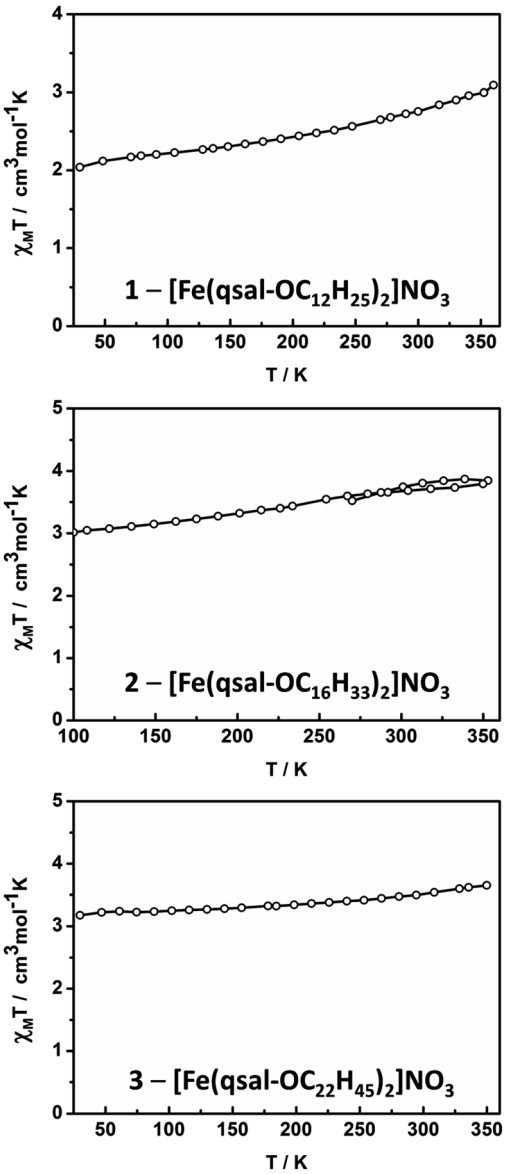

Fig. 5 $\chi_M T$ *vs.* T plots for **1–3**.

Open Access Article. Published on 10 September 2024. Downloaded on 8/18/2025 3:56:59 AM.
This article is licensed under a Creative Commons Attribution-NonCommercial 3.0 Unported Licence.

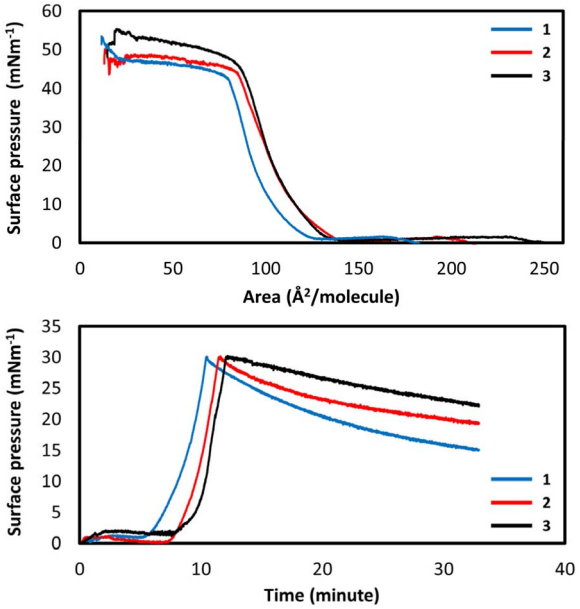

Fig. 6 Pressure–area isotherms (top) and stability measurements (bottom) for **1–3**.

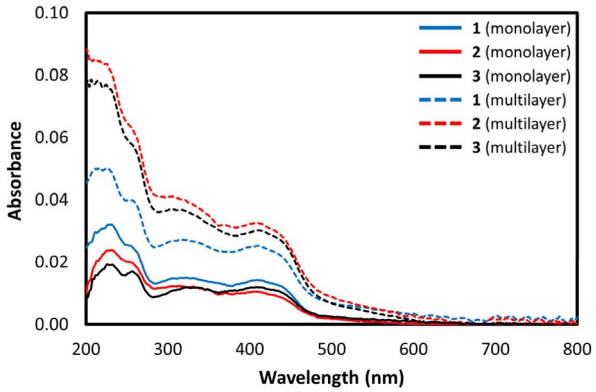

Fig. 7 UV-vis spectra of **1–3** as monolayer and multilayer films.

With successful monolayer formation, multi-layering studies were then carried out with emersion (up-stroke) of the slide being the first deposition. $[Fe(qsal\text{-}OC_{12}H_{25})_2]NO_3$ showed excellent transfer ratios (~1) for the first two layers (emersion and immersion), however the third layer (emersion) gave a transfer ratio of only 0.6. The overall result was a system that displayed Y-type film formation with successful deposition of a maximum of two layers. On moving to the longer chain $[Fe(qsal\text{-}OC_{16}H_{33})_2]NO_3$ complex the multi-layering ability was improved. This system displayed a maximum of three layers deposited in a Y-type film all with excellent transfer ratios of ~1 (Fig. 8). The longer chain $[Fe(qsal\text{-}OC_{22}H_{45})_2]NO_3$ system was also investigated for Y-type multi-layer film deposition and showed relatively poor deposition characteristics. Initial monolayer formation on emersion is good (transfer ratio ~1), however subsequent layers had lower transfer ratios (0.7 and 0.8 respectively) indicating that the optimal chain length from this

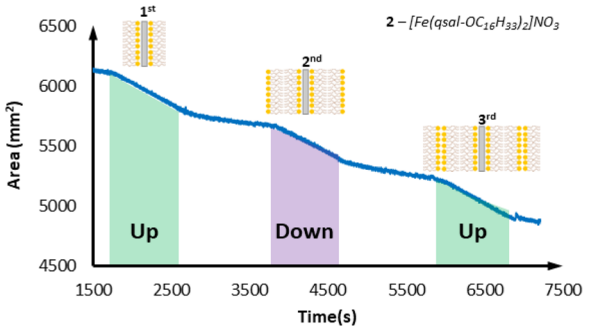

Fig. 8 Langmuir film transfer for $[Fe(qsal\text{-}OC_{16}H_{33})_2]NO_3$.

family is C_{16} (see Fig. S18 and S19 in ESI†). This may be due to back-folding with this longer alkyl chain, inhibiting the formation of the second layer.

UV-vis analysis of the mono- and multi-layered substrates indicated that the complexes remained intact on deposition as they had the same spectral features as was observed for the solution measurements. Multilayer films showed three absorption bands at 222 nm, 326, and 417 nm. The absorption band at 326 nm is assigned to the π–π* transition while the band at 417 nm, is assigned to the charge transfer band.

Conclusions

In this work, we successfully synthesized and characterized a novel class of alkylated $[Fe(qsal\text{-}OR)_2]NO_3$ complexes **1–3**. The solid-state structure of **1** reveals a bi-layer arrangement of the cationic complex, which is ideal for the formation of Langmuir–Blodgett film *via* self-assembly. The temperature dependent SQUID profile of **1–3** indicates that the integrating the long alkyl chain changes the packing leading to SCO compared with the trapped HS $[Fe(qsal\text{-}OMe)_2]NO_3$ complex in which R is methyl. Nevertheless, the profile is more gradual with the longer chain, contrasting the effect observed in $[Fe(4\text{-}OR\text{-}sal_2trien)]NO_3$. We can then demonstrate that all complexes can form a stable film and achieve reasonable transfer ratios to the glass surface, with **2** being the best in term of stability. Our results pave the way for the development of SCO devices with self-assembly on more diverse substrates currently being explored.

Experimental

General

Infrared spectra were recorded on a Bruker Tensor 27 FT-IR spectrometer with OPUS data collection program in the range of 400–4000 cm^{-1}, either as solid sample or KBr disc media. Electronic spectra were recorded at room temperature on either an Avantes Fiber Optics Spectrometer with Avalight-DHC and Avaspec ULS2048XL-USB2 in the range of 200–1000 nm or a PerkinElmer Lambda35 spectrometer in the range of 200–900 nm. The morphology of $[Fe(qsal\text{-}OR)_2]NO_3$ compounds were determined by Emission Scanning Electron Microscope (FESEM) at Walailak University, (JEOL JSM-7001 F, Zeiss Supra 55 VP, Zeiss Merlin Compact) operated at 3–5 kV. Samples were

© 2024 The Author(s). Published by the Royal Society of Chemistry

Open Access Article. Published on 10 September 2024. Downloaded on 8/18/2025 3:56:59 AM. This article is licensed under a Creative Commons Attribution-NonCommercial 3.0 Unported Licence.

placed on a carbon tape and coated with carbon. ^{1}H NMR spectra were recorded on a Bruker DPX400 NMR spectrometer at 300 K in $CDCl_3$. Chemical shifts are reported in parts per million and referenced to the residual solvent peak. Standard conventions indicating multiplicity were used: m = multiplet, t = triplet, d = doublet, s = singlet. Ar_q = signal originating from the quinoline ring and Ar_s = signal originating from the salicylic ring. ESI mass spectra were recorded using a MaXis (Bruker Daltonics, Germany) mass spectrometer equipped with a Time of Flight (TOF) analyser. Samples were introduced to the mass spectrometer *via* a Dionex Ultimate 3000 autosampler and uHPLC pump [Gradient 20% acetonitrile (0.2% formic acid) to 100% acetonitrile (0.2% formic acid) in five minutes at 0.6 mL min^{-1}. Column: Acquity UPLC BEH C18 (Waters) 1.7 micron 50 × 2.1 mm]. Langmuir studies: pressure–area isotherms and time stability were measured at 25 °C on a Kibron Micro-TroughXS (MTXS) Langmuir–Blodgett trough. Water for the subphase was purified with a Milli-Q Integral system (Millipore), and its resistivity was measured to be higher than 18 MΩ cm. Chloroform (HPLC grade, Fisher) was used as spreading solvent. Typically, drops (20 μL) of the surfactant solution (~0.5 mg mL^{-1}) were deposited using a microsyringe onto the subphase. After leaving the solvent to evaporate for ~10 min, the barriers were compressed at 7 mm min^{-1} and the surface pressure was monitored using a platinum DyneProbe that had been flamed. The quartz substrate for Langmuir–Blodgett deposition was treated with piranha solution prior to deposition.

X-ray crystallography and powder X-ray diffraction

Single-crystal X-ray diffraction data was either collected at 100 K on a Rigaku AFC12 goniometer equipped with an enhanced sensitivity (HG) Saturn 724+ detector mounted at the window of an FR-E+ Superbright Mo Kα rotating anode generator (λ = 0.71075 Å) with HF or VHF varimax optics, or a Rigaku 007 HF diffractometer equipped with an enhanced sensitivity Saturn 944+ detector with a Cu-Kα rotating anode generator (λ = 1.5418 Å) with HF varimax optics. Unit cell parameters were refined against all data and an empirical absorption correction applied in either CrystalClear[63] or CrysAlisPro.[64] All structures were solved by intrinsic phasing using SHELXT[65] and refined on F_0^2 by SHELXL using Olex2.[66] The CCDC nos. for Hqsal-$OC_{12}H_{25}$ and **1** are 2357075 and 2357074, respectively and can be downloaded free of charge at https://www.ccdc.cam.ac.uk/. X-ray diffraction patterns (XRD) were collected with a PANalytical Empyrean powder X-ray diffractometer operating at 45 kV and 40 mA. A standard Cu X-ray source was employed with a Kα1 wavelength of 1.5418 Å. Materials were scanned over a two-theta range of 5–80° with a 0.013° step size at a rate of 1.25° per minute. A beam knife was utilised to reduce background scattering at low angle two-theta.

Magnetic studies

Data were collected with a Quantum Design MPMS 5 SQUID magnetometer under an applied field of 1 T over the temperature range 30–350 K for **1–3**. The powdered or polycrystalline samples were placed in gel capsules and care was taken to allow long thermal equilibration times at each temperature. ^{1}H VT-NMR data were recorded on a Bruker DPX400 NMR spectrometer at 300 K in 0.5 mL THF, with 10 μL *t*-BuOH added. A reference solution of 10 μL *t*-BuOH in 50 μL THF was prepared in a small glass capillary.

Synthesis and characterization

Synthesis of [Fe(qsal-$OC_{12}H_{25}$)$_2$]NO_3. A solution of Hqsal-$OC_{12}H_{25}$ (0.64 g, 1.5 mmol) in DCM (10 mL) was added to a solution of iron(III) nitrate nonahydrate (0.30 g, 0.75 mmol) in methanol (2 mL) and stirred for 10 minutes. Triethylamine (208 μL, 1.50 mmol) was added to the mixture, which was stirred for 1 h and then evaporated to give a black solid. After this, the solid was dissolved in DCM (20 mL) and dry-loaded to the short pad of Al_2O_3. The pad was eluted with DCM : Et_2O (1 : 1, 50 mL) under vacuum to remove organic impurity, followed by ethanol : THF (2 : 1, 250 mL) to collect the product. The resulting black solution was evaporated to dryness giving the complex as a black solid (0.49 g, 68%). Found (calcd%) for $C_{56}H_{70}FeN_5O_7$ (981.03 g mol^{-1}): C 68.27 (68.56), H 7.18 (7.19), N 7.07 (7.14). HRMS (ESI+) *m*/*z* 918.47 [M–NO_3]$^+$ (Calcd for [Fe(qsal-$OC_{12}H_{25}$)$_2$]$^+$, 918.47). UV/vis, λ_{max} (MeOH)/nm 325 (ε/dm^3 mol^{-1} cm^{-1} 17 175) and 403 (18 845). FT-IR, ν_{max}/cm^{-1} 2945, 2920, 2851 (alkyl chain), 1597 (C=N), 1379 (NO from anion).

Synthesis of [Fe(qsal-$OC_{16}H_{33}$)$_2$]NO_3. A solution of Hqsal-$OC_{16}H_{33}$ (0.38 g, 0.77 mmol) in DCM (10 mL) was added to a solution of iron(III) nitrate nonahydrate (0.16 g, 0.38 mmol) in methanol (2 mL) for 15 minutes. Triethylamine (106 μL, 0.77 mmol) was added in the mixture, which was stirred for 2 h and then evaporated to give a black solid. After this, the solid (0.41 g) was dissolved in DCM (20 mL) and dry-loaded to the short pad of Al_2O_3. The pad was eluted with DCM : Et_2O (1 : 1, 50 mL) under vacuum to remove organic impurity, followed by ethanol : THF (2 : 1, 250 mL) to collect the product. The resulting black solution was evaporated to dryness giving the complex as a black solid (0.22 g, 54% for flash chromatography). Found (calcd%) for $C_{64}H_{86}FeN_5O_7$ (1093.24 g mol^{-1}): C 70.05 (70.31), H 7.58 (7.93), N 6.50 (6.41). HRMS (ESI+) *m*/*z* 1030.60 [M–NO_3]$^+$ (Calcd for [Fe(qsal-$OC_{16}H_{33}$)$_2$]$^+$, 1030.60). UV/vis, λ_{max} (MeOH)/nm 325 (ε/dm^3 mol^{-1} cm^{-1} 20 100) and 403 (21 135). FT-IR, ν_{max}/cm^{-1} 2945, 2920, 2851 (alkyl chain), 1599 (C=N), 1379 (NO from anion).

Synthesis of [Fe(qsal-$OC_{22}H_{45}$)$_2$]NO_3. A solution of Hqsal-$OC_{22}H_{45}$ (0.57 g, 1.0 mmol) in DCM (10 mL) was added to a solution of iron(III) nitrate nonahydrate (0.20 g, 0.5 mmol) in methanol (2 mL) for 10 minutes. Triethylamine (138 μL, 1.0 mmol) was added in the mixture, which was stirred for 1 h and then evaporated to give a black solid. The solid was washed with hexane and then dissolved in EtOH–THF (2 : 1, 45 mL) and filtered through Al_2O_3. A further washing with EtOH–THF (2 : 1, 30 mL) and evaporation gave the complex as a as a black solid (0.46 g, 74%). Found (calcd%) for $C_{76}H_{110}FeN_5O_7$ (1261.56 g mol^{-1}): C 72.09 (72.36) H 7.86 (7.93), N 5.31 (5.55). HRMS (ESI+) *m*/*z* 1189.79 [M–NO_3]$^+$ (Calcd for [Fe(qsal-$OC_{22}H_{45}$)$_2$]$^+$, 1189.79). UV/vis, λ_{max}(MeOH)/nm ε/dm^3 mol^{-1} cm^{-1} 325 (21 805) and 403

Open Access Article. Published on 10 September 2024. Downloaded on 8/18/2025 3:56:59 AM. This article is licensed under a Creative Commons Attribution-NonCommercial 3.0 Unported Licence.

(22 360). FT-IR, ν_{max}/cm^{-1} 2941, 2916, 2849 (alkyl chain), 1597 (C=N), 1379 (NO from anion).

Data availability

The data supporting this article have been included as part of the ESI.† The CCDC no. for Hqsal-$OC_{12}H_{25}$ and **1** are 2357075 and 2357074, respectively.

Conflicts of interest

There are no conflicts to declare.

Acknowledgements

This research has received funding support from the NSRF *via* the Program Management Unit for Human Resources & Institutional Development, Research and Innovation (Grant Number: B39G670018). The Development and Promotion of Science and Technology Talents project is thanked for a scholarship to P. P. The University of Auckland Shared Research Equipment Platform (ShaRe) and Dr Timothy Christopher for collecting powder X-ray diffraction data.

Notes and references

1 M. A. Halcrow, *Spin-Crossover Materials: Properties and Applications*, 2013.
2 A. Enriquez-Cabrera, A. Rapakousiou, M. Piedrahita Bello, G. Molnár, L. Salmon and A. Bousseksou, *Coord. Chem. Rev.*, 2020, **419**, 213396.
3 P. Gütlich, Y. Garcia and H. A. Goodwin, *Chem. Soc. Rev.*, 2000, **29**, 419–427.
4 M. Nihei, T. Shiga, Y. Maeda and H. Oshio, *Coord. Chem. Rev.*, 2007, **251**, 2606–2621.
5 A. B. Gaspar, M. Seredyuk and P. Gütlich, *J. Mol. Struct.*, 2009, **924–926**, 9–19.
6 D. J. Harding, P. Harding and W. Phonsri, *Coord. Chem. Rev.*, 2016, **313**, 38–61.
7 S. Hayami, K. Hiki, T. Kawahara, Y. Maeda, D. Urakami, K. Inoue, M. Ohama, S. Kawata and O. Sato, *Chem.–Eur. J.*, 2009, **15**, 3497–3508.
8 S. Hayami, Z. Z. Gu, H. Yoshiki, A. Fujishima and O. Sato, *J. Am. Chem. Soc.*, 2001, **123**, 11644–11650.
9 S. Hayami, T. Kawahara, G. Juhász, K. Kawamura, K. Uehashi, O. Sato and Y. Maeda, *J. Radioanal. Nucl. Chem.*, 2003, **255**, 443–447.
10 M. Shatruk, H. Phan, B. A. Chrisostomo and A. Suleimenova, *Coord. Chem. Rev.*, 2015, **289–290**, 62–73.
11 E. Trzop, D. Zhang, L. Piñeiro-Lopez, F. J. Valverde-Muñoz, M. Carmen Muñoz, L. Palatinus, L. Guerin, H. Cailleau, J. A. Real and E. Collet, *Angew. Chem., Int. Ed.*, 2016, **55**, 8675–8679.
12 Z. Y. Li, H. Ohtsu, T. Kojima, J. W. Dai, T. Yoshida, B. K. Breedlove, W. X. Zhang, H. Iguchi, O. Sato, M. Kawano and M. Yamashita, *Angew. Chem., Int. Ed.*, 2016, **55**, 5184–5189.
13 Y. Meng, Q. Q. Sheng, M. N. Hoque, Y. C. Chen, S. G. Wu, J. Tucek, R. Zboril, T. Liu, Z. P. Ni and M. L. Tong, *Chem.–Eur. J.*, 2017, **23**, 10034–10037.
14 C. Zheng, S. Jia, Y. Dong, J. Xu, H. Sui, F. Wang and D. Li, *Inorg. Chem.*, 2019, **58**, 14316–14324.
15 F. F. Martins, A. Joseph, H. P. Diogo, M. E. Minas da Piedade, L. P. Ferreira, M. D. Carvalho, S. Barroso, M. J. Romão, M. J. Calhorda and P. N. Martinho, *Eur. J. Inorg. Chem.*, 2018, **2018**, 2976–2983.
16 Z. Y. Li, J. W. Dai, Y. Shiota, K. Yoshizawa, S. Kanegawa and O. Sato, *Chem.–Eur. J.*, 2013, **19**, 12948–12952.
17 M. Griffin, S. Shakespeare, H. J. Shepherd, C. J. Harding, J. F. Létard, C. Desplanches, A. E. Goeta, J. A. K. Howard, A. K. Powell, V. Mereacre, Y. Garcia, A. D. Naik, H. Müller-Bunz and G. G. Morgan, *Angew. Chem., Int. Ed.*, 2011, **50**, 896–900.
18 T. Boonprab, S. J. Lee, S. G. Telfer, K. S. Murray, W. Phonsri, G. Chastanet, E. Collet, E. Trzop, G. N. L. Jameson, P. Harding and D. J. Harding, *Angew. Chem., Int. Ed.*, 2019, **58**, 11811–11815.
19 D. J. Harding, D. Sertphon, P. Harding, K. S. Murray, B. Moubaraki, J. D. Cashion and H. Adams, *Chem.–Eur. J.*, 2013, **19**, 1082–1090.
20 D. J. Harding, W. Phonsri, P. Harding, K. S. Murray, B. Moubaraki and G. N. L. Jameson, *Dalton Trans.*, 2014, **44**, 15079–15082.
21 N. Phukkaphan, D. L. Cruickshank, K. S. Murray, W. Phonsri, P. Harding and D. J. Harding, *Chem. Commun.*, 2017, **53**, 9801–9804.
22 B. J. C. Vieira, J. C. Dias, I. C. Santos, L. C. J. Pereira, V. Da Gama and J. C. Waerenborgh, *Inorg. Chem.*, 2015, **54**, 1354–1362.
23 S. Brooker, *Chem. Soc. Rev.*, 2015, **44**, 2880–2892.
24 K. Fukuroi, K. Takahashi, T. Mochida, T. Sakurai, H. Ohta, T. Yamamoto, Y. Einaga and H. Mori, *Angew. Chem., Int. Ed.*, 2014, **53**, 1983–1986.
25 M. Nakaya, R. Ohtani, L. F. Lindoy and S. Hayami, *Inorg. Chem. Front.*, 2021, **8**, 484–498.
26 R. Díaz-Torres, G. Chastanet, E. Collet, E. Trzop, P. Harding and D. J. Harding, *Chem. Sci.*, 2023, **14**, 7185–7191.
27 R. Díaz-Torres, T. Boonprab, S. Gómez-Coca, E. Ruiz, G. Chastanet, P. Harding and D. J. Harding, *Inorg. Chem. Front.*, 2022, 22–24.
28 W. Phonsri, P. Harding, L. Liu, S. G. Telfer, K. S. Murray, B. Moubaraki, T. M. Ross, G. N. L. Jameson and D. J. Harding, *Chem. Sci.*, 2017, **8**, 3949–3959.
29 D. Sertphon, D. J. Harding, P. Harding, K. S. Murray, B. Moubaraki, H. Adams, A. Alkaş and S. G. Telfer, *Eur. J. Inorg. Chem.*, 2016, **2016**, 432–438.
30 R. Díaz-Torres, W. Phonsri, K. S. Murray, P. Harding and D. J. Harding, *Cryst. Growth Des.*, 2022, **22**, 1543–1547.
31 B. J. C. Vieira, L. C. J. Pereira, V. da Gama and J. C. Waerenborgh, *CrystEngComm*, 2023, **25**, 6472–6477.
32 R. Diáz-Torres, W. Phonsri, K. S. Murray, L. Liu, M. Ahmed, S. M. Neville, P. Harding and D. J. Harding, *Inorg. Chem.*, 2020, **59**, 13784–13791.

© 2024 The Author(s). Published by the Royal Society of Chemistry

Open Access Article. Published on 10 September 2024. Downloaded on 8/18/2025 3:56:59 AM. This article is licensed under a Creative Commons Attribution-NonCommercial 3.0 Unported Licence.

33 S. Zhao, H. Zhou, C.-Y. Qin, H.-Z. Zhang, Y.-H. Li, M. Yamashita and S. Wang, *Chem.–Eur. J.*, 2023, **29**, e202300554.
34 I. R. Jeon, O. Jeannin, R. Clérac, M. Rouzières and M. Fourmigué, *Chem. Commun.*, 2017, **53**, 4989–4992.
35 B. J. C. Vieira, L. C. J. Pereira, V. da Gama, I. C. Santos, A. C. Cerdeira and J. C. Waerenborgh, *Magnetochemistry*, 2022, **8**, 1–19.
36 P. N. Martinho, C. J. Harding, H. Müller-Bunz, M. Albrecht and G. G. Morgan, *Eur. J. Inorg. Chem.*, 2010, 675–679.
37 C. Gandolfi, G. G. Morgan and M. Albrecht, *Dalton Trans.*, 2012, **41**, 3726–3730.
38 C. Gandolfi, N. Miyashita, D. G. Kurth, P. N. Martinho, G. G. Morgan and M. Albrecht, *Dalton Trans.*, 2010, **39**, 4508–4516.
39 P. Coronel, A. Barraud, R. Claude, O. Kahn, A. Ruaudel-Teixier and J. Zarembowitch, *J. Chem. Soc., Chem. Commun.*, 1989, 193–194.
40 H. Soyer, E. Dupart, C. Mingotaud, C. J. Gomez-Garcia and P. Delhaès, *Colloids Surf., A*, 2000, **171**, 275–282.
41 A. Ruaudel-Teixier, A. Barraud, P. Coronel and O. Kahn, *Thin Solid Films*, 1988, **160**, 107–115.
42 N. G. White, H. L. C. Feltham, C. Gandolfi, M. Albrecht and S. Brooker, *Dalton Trans.*, 2010, **39**, 3751–3758.
43 Y. Bodenthin, U. Pietsch, H. Möhwald and D. G. Kurth, *J. Am. Chem. Soc.*, 2005, **127**, 3110–3114.
44 H. Soyer, C. Mingotaud, M. L. Boillot and P. Delhaes, *Langmuir*, 1998, **14**, 5890–5894.
45 O. Roubeau, B. Agricole, R. Clérac and S. Ravaine, *J. Phys. Chem. B*, 2004, **108**, 15110–15116.
46 J. T. Culp, J. H. Park, D. Stratakis, M. W. Meisel and D. R. Talham, *J. Am. Chem. Soc.*, 2002, **124**, 10083–10090.
47 J. Weihermüller, S. Schlamp, W. Milius, F. Puchtler, J. Breu, P. Ramming, S. Hüttner, S. Agarwal, C. Göbel, M. Hund, G. Papastavrou and B. Weber, *J. Mater. Chem. C*, 2019, **7**, 1151–1163.
48 S. Sundaresan, J. A. Kitchen and S. Brooker, *Inorg. Chem. Front.*, 2020, **7**, 2050–2059.
49 J. A. Kitchen, N. G. White, C. Gandolfi, M. Albrecht, G. N. L. Jameson, J. L. Tallon and S. Brooker, *Chem. Commun.*, 2010, **46**, 6464–6466.
50 R. Akiyoshi, Y. Hirota, D. Kosumi, M. Tsutsumi, M. Nakamura, L. F. Lindoy and S. Hayami, *Chem. Sci.*, 2019, **10**, 5843–5848.
51 I. Galadzhun, R. Kulmaczewski, N. Shahid, O. Cespedes, M. J. Howard and M. A. Halcrow, *Chem. Commun.*, 2021, **57**, 4039–4042.
52 H. L. C. Feltham, C. Johnson, A. B. S. Elliott, K. C. Gordon, M. Albrecht and S. Brooker, *Inorg. Chem.*, 2015, **54**, 2902–2909.
53 Y. Guo, A. Rotaru, H. Müller-Bunz, G. G. Morgan, S. Zhang, S. Xue and Y. Garcia, *Dalton Trans.*, 2021, **50**, 12835–12842.
54 D. Rosario-Amorin, P. Dechambenoit, A. Bentaleb, M. Rouzières, C. Mathonière and R. Clérac, *J. Am. Chem. Soc.*, 2018, **140**, 98–101.
55 M. Seredyuk, M. C. Muñoz, V. Ksenofontov, P. Gütlich, Y. Galyametdinov and J. A. Real, *Inorg. Chem.*, 2014, **53**, 8442–8454.
56 Q. Zhao, J. P. Xue, Z. K. Liu, Z. S. Yao and J. Tao, *Dalton Trans.*, 2021, **50**, 11106–11112.
57 R. Akiyoshi, R. Ohtani, L. F. Lindoy and S. Hayami, *Dalton Trans.*, 2021, **50**, 5065–5079.
58 R. Akiyoshi, K. Kuroiwa, S. Alao Amolegbe, M. Nakaya, R. Ohtani, M. Nakamura, L. F. Lindoy and S. Hayami, *Chem. Commun.*, 2017, **53**, 4685–4687.
59 Y. Komatsu, K. Kato, Y. Yamamoto, H. Kamihata, Y. H. Lee, A. Fuyuhiro, S. Kawata and S. Hayami, *Eur. J. Inorg. Chem.*, 2012, 2769–2775.
60 C. Gandolfi, C. Moitzi, P. Schurtenberger, G. G. Morgan and M. Albrecht, *J. Am. Chem. Soc.*, 2008, **130**, 14434–14435.
61 H. L. C. Feltham, A. S. Barltrop and S. Brooker, *Coord. Chem. Rev.*, 2017, **344**, 26–53.
62 M. Bodik, M. Jergel, E. Majkova and P. Siffalovic, *Adv. Colloid Interface Sci.*, 2020, **283**, 102239.
63 Rigaku Oxford Diffraction CrystalClear-SM Expert 3.1. 2012.
64 Rigaku Oxford Diffraction, CrysAlisPro v1.171.39.34 2017.
65 G. M. Sheldrick, *Acta Crystallogr., Sect. A: Found. Adv.*, 2015, **71**, 3–8.
66 G. M. Sheldrick, *Acta Crystallogr., Sect. C: Struct. Chem.*, 2015, **71**, 3–8.

© 2024 The Author(s). Published by the Royal Society of Chemistry